Electron-cyclotron wave propagation, absorption and current drive in the presence of neoclassical tearing modes

2012 Plasma Phys. Control. Fusion 54 095005

(http://iopscience.iop.org/0741-3335/54/9/095005)

IOP Publishing Plasma Physics and Controlled Fusion

Plasma Phys. Control. Fusion **54** (2012) 095005 (12pp) doi:10.1088/0741-3335/54/9/095005

Electron-cyclotron wave propagation, absorption and current drive in the presence of neoclassical tearing modes

Heinz Isliker[1], Ioanna Chatziantonaki[1], Christos Tsironis[1,2] and Loukas Vlahos[1]

[1] Section of Astrophysics, Astronomy and Mechanics, Department of Physics, Association Euratom-Hellenic Republic, Aristotle University of Thessaloniki, 54 124 Thessaloniki, Greece
[2] School of Electrical and Computer Engineering, National Technical University of Athens, 157 73 Athens, Greece

Received 4 October 2011, in final form 29 May 2012
Published 27 July 2012
Online at stacks.iop.org/PPCF/54/095005

Abstract
We analyze the propagation of electron-cyclotron waves, their absorption and current drive when neoclassical tearing modes (NTMs), in the form of magnetic islands, are present in a tokamak plasma. So far, the analysis of the wave propagation and power deposition in the presence of NTMs has been performed mainly in the frame of an axisymmetric magnetic field, ignoring any effects from the island topology. Our analysis starts from an axisymmetric magnetic equilibrium, which is perturbed such as to exhibit magnetic islands. In this geometry, we compute the wave evolution with a ray-tracing code, focusing on the effect of the island topology on the efficiency of the absorption and current drive. To increase the precision in the calculation of the power deposition, the standard analytical flux-surface labeling for the island region has been adjusted from the usual cylindrical to toroidal geometry. The propagation up to the O-point is found to be little affected by the island topology, whereas the power absorbed and the driven current are significantly enhanced, because the resonant particles are bound to the small volumes in between the flux surfaces of the island. The consequences of these effects on the NTM evolution are investigated in terms of the modified Rutherford equation.

1. Introduction

Neoclassical tearing modes (NTMs) often limit the performance of tokamak plasmas, because the magnetic islands they generate bring down the plasma energy and the angular momentum, leading to loss of confinement or even disruption [1–3]. An NTM is sustained by a helical bootstrap current and can grow to a large amplitude due to the amplification effect of the bootstrap current on an initially small magnetic island ('seed' island). The upper limit for the plasma pressure is imposed by the ideal non-axisymmetric kink modes and by the resistive TMs, which break the magnetic flux surfaces on which the safety factor q assumes rational values, $q = m/n$, where m, n are the poloidal and toroidal mode number, respectively (the reader is referred to [4] for details).

A classical TM is linearly unstable when the plasma current profile is unstable, therefore the TM is of lower energy than the initial state, and it is also non-axisymmetric due to the presence of islands. On the other hand, the NTM is a high-beta effect that can occur even when the plasma is classically stable [1]. In a toroidal plasma, a poloidal non-uniformity of the axi-symmetric magnetic field leads to the appearance of a trapped particle population, and the passing electrons reach an equilibrium with velocities determined by the collisions with the ions and the trapped electrons. The bootstrap current, carried by the passing electrons, can be a significant part of the total current parallel to the magnetic field when the plasma pressure is high [5]. When the safety factor increases monotonically with the minor radius and the plasma pressure decreases, then a helical perturbation leads to the degradation of the pressure and thus has a destabilizing effect.

It is estimated that the NTMs will be dynamically unstable at ITER, since a high plasma pressure is required for an effective fusion device, and that both, the (2, 1) and the (3, 2) mode, respectively, will appear [6]. Various techniques are

under development for the stabilization and the passive or active control of these unstable modes. The main methods include (a) the use of helical magnetic fields to restrain the perturbed bootstrap currents and (b) the replacement of the lacking bootstrap current through the application of localized electron-cyclotron current drive (ECCD). Among these, the ECCD compensation of the missing bootstrap current is considered to be the most effective method for NTM stabilization. The suppression and control of NTMs with ECCD has been demonstrated in several experiments in the last years, such as ASDEX upgrade, DIII-D and JT-60U [7].

Many authors have studied the characteristics of the NTM stabilization by ECCD, investigating the effect of localized EC power deposition and current drive in magnetic islands (comprehensive reviews on this subject are [2, 8]). The evolution of ECCD-driven magnetic islands has been extensively investigated in terms of the modified Rutherford equation, a modification of the classical Rutherford equation for TMs with the inclusion of (among other effects) the bootstrap current, the polarization current and the ECCD [7, 9]. It has been pointed out that, in order to succeed in a more effective mode stabilization, the driven current (and therefore the EC resonance) should be highly localized around the O-point, and its direction should be aligned with the equilibrium bootstrap current. Furthermore, the possible advantage of early application of ECCD has been pointed out and is under current research [10].

In the theory of plasma waves, a number of methods has been developed for the computation of the wave propagation, the resonant absorption and the wave-induced electric current. For the wave propagation, most applications are based on the asymptotic methods originating from geometric optics (GO) [11, 12]: ray tracing, quasi-optics and beam tracing. In ray-tracing, Hamiltonian equations provide the position and the wave-number along the ray trajectory via the derivatives of the dispersion relation [12]. The rays do not interact among themselves, therefore wave effects such as diffraction are not taken into account. In quasi-optics, a Gaussian beam is simulated in terms of interacting rays, so that the basic wave effects are preserved [13]. Beam tracing is a more convenient description based on a combination of ray tracing with a set of functions for the evolution of the beam width and the wave-front curvature [14]. It is important to underline that GO should be applied only when the wavelength is much smaller than the plasma inhomogeneity length scale, which is a valid approximation in most cases of interest of tokamak wave propagation.

The absorption of the wave is usually calculated either by evaluating the linear absorption coefficient along the ray path [15] or by solving a Fokker–Planck (F–P) equation for the velocity distribution function in the quasilinear approximation. The driven current can be calculated analytically in terms of the linear adjoint method [16], or, in the quasilinear approximation, from the first moment of the distribution function, as given by the solution of the velocity-space F–P equation [17]. There is a number of sophisticated codes implementing the above schemes, and the results in some cases are in sufficient agreement with the experiments (for details on these methods and codes see [18] and references therein).

In the majority of models for the simulation of ECCD-based NTM stabilization, the analysis of the wave propagation and power deposition was performed in the framework of the unperturbed, axisymmetric magnetic topology, taking into account only the (rational-q) flux surface of interest while ignoring any effects from the islands. Such a simplified treatment is justified by the fact that the amplitude of the perturbation that generates the islands in most cases is very small compared with the background magnetic field. However, the magnetic island topology introduces significant changes in the magnetic field and the plasma profiles compared with the axisymmetric case, namely a flattening of the density and temperature profiles within the island region, and a different nesting of the flux surfaces, which may play a crucial role in the wave deposition. Moreover, recent studies have shown that the current drive efficiency in the presence of islands may be much different from the axisymmetric case, which has led to different estimates of the minimum ECCD required for NTM stabilization [19–21].

In this work, we study the EC propagation, absorption and current drive in the presence of NTMs, using a ray-tracing numerical code and a plasma magnetic field configuration that includes magnetic islands. In the context of the current drive requirements for NTM stabilization in modern tokamaks, we focus on the effect of the magnetic island topology on the efficiency of the wave absorption and current drive through (i) the magnetic field perturbation itself, (ii) the flattening of the radial profiles of the plasma parameters (density, temperature) within the island region and (iii) the morphology and the volumes of the perturbed flux surfaces, into which the wave energy is deposited. To increase the precision in the calculation of the flux-surface volumes, the standard analytical flux-surface labeling has been adjusted from the usual cylindrical to toroidal coordinates. The connection of the results to the dynamics of the NTM stabilization by ECCD is formulated in terms of the modified Rutherford equation.

This paper is structured as follows: in section 2, we introduce an analytic, non-axisymmetric magnetic configuration from a combination of an axisymmetric equilibrium with an NTM-like perturbation in the poloidal flux, and we also present a labeling of the flux surfaces within the island region for toroidal coordinates. In section 3, we give an extended description of the used ray-tracing numerical scheme, which includes the determination of the volumes in the island topology. The main results are presented in section 4, and in section 5 the implications of these results for the NTM dynamical evolution are shown. Finally, the last section contains a discussion of the main conclusions and the limitations of our model.

2. Analytic description of the perturbed magnetic equilibrium

In order to derive a realistic analytical model for the tokamak magnetic equilibrium and the island geometry, we make use of the Clebsch form for the magnetic field [22],

$$\boldsymbol{B} = \nabla\psi_{\mathrm{t}} \times \nabla\theta + \nabla\varphi \times \nabla\psi_{\mathrm{p}}, \tag{1}$$

which is expressed in the curvilinear toroidal coordinate system (r, θ, φ), with r the radial coordinate in the poloidal cross section of the torus (usually called the minor radius, with maximum value α), θ the poloidal angle, and φ the toroidal angle, and where ψ_p and ψ_t are the poloidal and the toroidal flux functions, respectively (in Weber units).

To obtain a more explicit expression than equation (1) for the magnetic field, we consider ψ_t and ψ_p as functions of r, θ, φ, so that

$$\nabla\psi_\mathrm{p} = \partial_r\psi_\mathrm{p}\,\nabla r + \partial_\theta\psi_\mathrm{p}\,\nabla\theta + \partial_\varphi\psi_\mathrm{p}\,\nabla\varphi,$$
$$\nabla\psi_\mathrm{t} = \partial_r\psi_\mathrm{t}\,\nabla r + \partial_\theta\psi_\mathrm{t}\,\nabla\theta + \partial_\varphi\psi_\mathrm{t}\,\nabla\varphi.$$

Inserting the above equations into equation (1) and transforming to orthonormal toroidal coordinates with unit base vectors $\boldsymbol{e}_{\hat{r}}$, $\boldsymbol{e}_{\hat{\theta}}$, $\boldsymbol{e}_{\hat{\varphi}}$, one obtains

$$\boldsymbol{B} = -(\partial_\theta\psi_\mathrm{p} + \partial_\varphi\psi_\mathrm{t})\,\frac{1}{rR}\,\boldsymbol{e}_{\hat{r}} + \partial_r\psi_\mathrm{p}\,\frac{1}{R}\,\boldsymbol{e}_{\hat{\theta}} + \frac{1}{r}\,\partial_r\psi_\mathrm{t}\,\boldsymbol{e}_{\hat{\varphi}}, \quad (2)$$

with $R = R_0 + r\cos\theta$ (R_0 is the major radius). The Cartesian components of the magnetic field can in turn be derived by substituting in equation (2) the unit vectors $\boldsymbol{e}_{\hat{r}}$, $\boldsymbol{e}_{\hat{\theta}}$, $\boldsymbol{e}_{\hat{\varphi}}$ with their Cartesian expressions,

$$B_x = -\frac{1}{rR}\cos\theta\cos\varphi\left(\frac{\partial\psi_\mathrm{p}}{\partial\theta} + \frac{\partial\psi_\mathrm{t}}{\partial\varphi}\right) - \frac{1}{R}\sin\theta\cos\varphi\frac{\partial\psi_\mathrm{p}}{\partial r} - \frac{1}{r}\sin\varphi\frac{\partial\psi_\mathrm{t}}{\partial r}, \quad (3a)$$

$$B_y = -\frac{1}{rR}\cos\theta\sin\varphi\left(\frac{\partial\psi_\mathrm{p}}{\partial\theta} + \frac{\partial\psi_\mathrm{t}}{\partial\varphi}\right) - \frac{1}{R}\sin\theta\sin\varphi\frac{\partial\psi_\mathrm{p}}{\partial r} + \frac{1}{r}\cos\varphi\frac{\partial\psi_\mathrm{t}}{\partial r}, \quad (3b)$$

$$B_z = -\frac{1}{rR}\sin\theta\left(\frac{\partial\psi_\mathrm{p}}{\partial\theta} + \frac{\partial\psi_\mathrm{t}}{\partial\varphi}\right) + \frac{1}{R}\cos\theta\frac{\partial\psi_\mathrm{p}}{\partial r}. \quad (3c)$$

2.1. The background equilibrium magnetic field

Regarding the axisymmetric part of the magnetic field, corresponding to the background equilibrium, a very convenient and widely used representation is what can be called the 'vacuum magnetic field' [23, 24]

$$B_\mathrm{t}(r,\theta) = \frac{B_0}{1+\epsilon_\mathrm{A}(r)\cos\theta}, \quad (4a)$$

$$B_\mathrm{p}(r,\theta) = \frac{\epsilon_\mathrm{A}(r)}{q\,(r)}B_\mathrm{t}(r), \quad (4b)$$

where B_t, B_p are the toroidal and poloidal components, respectively, B_0 is the toroidal field on the magnetic axis, $\epsilon_\mathrm{A}(r) = r/R_0$ is the inverse aspect ratio for an arbitrary radial position r and $q(r) = \mathrm{d}\varphi/\mathrm{d}\theta$ is the safety factor.

A straightforward way to determine the flux functions ψ_t, ψ_p in equations (2) and (3*a*)–(3*c*) is to use the relation

$$\frac{1}{r}\partial_r\psi_\mathrm{t} = B_\varphi \quad (5)$$

from equation (2), and on demanding that $B_\varphi \equiv B_\mathrm{t}$, with B_t from equations (4*a*), one finds by simple integration

$$\psi_\mathrm{t} = \frac{R_0 B_0}{\cos^2\theta}\left[r\cos\theta - R_0\ln\frac{R}{R_0}\right]. \quad (6)$$

We note here that the simplifying assumption $\psi_\mathrm{t} = r^2/a^2$ for the toroidal flux, which is often made in the literature, is actually connected to the large aspect ratio approximation ($r/R \ll 1$) and yields a much less realistic toroidal field with $B_\varphi = \mathrm{const}$, whereas the toroidal field used in this work has the characteristic $1/R$ dependence.

The singularity in equation (6) at $\cos\theta = 0$ is actually not a real one, since a Taylor series expansion of the logarithm involved in the equation yields

$$\psi_\mathrm{t} \approx B_0\left[\frac{1}{2}r^2 - \frac{1}{3R_0}r^3\cos\theta\right], \qquad |\cos\theta| \ll 1, \quad (7)$$

which is finite at $\cos\theta = 0$. Regarding the computation of the background part $\psi_{\mathrm{p}0}$ of the poloidal flux function, again from equation (2) one has that

$$\frac{1}{R}\frac{\partial\psi_\mathrm{p}}{\partial r} = B_\theta, \quad (8)$$

so that the choice

$$\psi_{\mathrm{p}0} = B_0\int \mathrm{d}\sigma/q(r(\sigma)), \quad (9)$$

with $\sigma = r^2/2$, obviously yields $B_\theta \equiv B_\mathrm{p}$ in equations (4*b*), as intended.

Following [25], a monotonically increasing safety factor is assumed,

$$q\,(\chi) = \frac{4}{(2-\chi)\left(2-2\chi+\chi^2\right)}, \quad (10)$$

with $\chi = r^2/\alpha^2$, so that $q(0) = 1$ at the magnetic axis and $q(\alpha) = 4$ at the edge. With this form of q, $\psi_{\mathrm{p}0}$ (equation (9)) can be determined analytically,

$$\psi_{\mathrm{p}0} = \frac{B_0}{4}\left(2r^2 - \frac{3}{2}\frac{r^4}{a^2} + \frac{2}{3}\frac{r^6}{a^4} - \frac{1}{8}\frac{r^8}{a^6}\right). \quad (11)$$

2.2. The NTM-like perturbations

Magnetic islands appear at flux surfaces where the safety factor assumes rational values, $q(r_\mathrm{s}) = m/n$, with r_s the radial position of the resonant surface and m, n integers indicating the number of toroidal and poloidal windings, respectively, after which the magnetic field lines close on themselves ([3], section 7.2 in [26]). For the investigation of the effect of islands on the wave propagation and absorption, we use a model for the local magnetic field structure of magnetic islands, and in order to preserve the divergence freeness of the magnetic field, we formulate the island topology as a perturbation $\psi_{\mathrm{p}1}$ to the background poloidal flux $\psi_{\mathrm{p}0}$, which together serve as a potential ψ_p in equations (2) and (3*a*)–(3*c*),

$$\psi_\mathrm{p} = \psi_{\mathrm{p}0} + \psi_{\mathrm{p}1}. \quad (12)$$

Following [27, Chapter 9] and [28], the perturbation can be represented as

$$\psi_{\mathrm{p}1} = \psi_{\mathrm{p}1}\,(\psi_\mathrm{t}, \theta, \varphi) = \varepsilon_{mn}(r)\cos\left(m\theta - n\varphi\right), \quad (13)$$

for an excited (m, n)-mode. A self-consistent expression for $\varepsilon_{mn}(r)$ is given in [29], for our purposes though it is sufficient to use the low-order approximation given in [30],

$$\psi_{\mathrm{p1}} = \psi_{\mathrm{p1}}(r, \theta, \varphi) = -\frac{r}{m}\varepsilon_{mn}^{(0)}\left(1 + \frac{r - r_{\mathrm{s}}}{\alpha_{\pm}}\right)\cos(m\theta - n\varphi), \tag{14}$$

with $\alpha_{\pm}$ the slopes, where the subscripts '+' and '-' are for $r > r_{\mathrm{s}}$ and $r < r_{\mathrm{s}}$, respectively, and $\varepsilon_{mn}^{(0)}$ the perturbation strengths. In this form, radial asymmetries can be taken into account (see also [31]), they do though not play an important role for the purposes of our study, so that we will assume $\alpha_{+} = \alpha_{-}$ for simplicity.

From equations (2) and (14), the radial magnetic field is

$$B_r = -\frac{1}{R}\varepsilon_{mn}^{(0)}\left(1 + \frac{r - r_{\mathrm{s}}}{\alpha_{\pm}}\right)\sin(\xi), \tag{15}$$

with $\xi = m\theta - n\varphi$ a helical coordinate (i.e. in the direction perpendicular to the line through the island's O-point), and since ψ_{p1} depends on r, we also have a perturbation term $B_{\theta 1}$ in the poloidal field, according to equations (2) and (14),

$$B_\theta = B_{\theta 0} + B_{\theta 1} = B_{\theta 0} - \frac{1}{Rm}\varepsilon_{mn}^{(0)}\left(1 + \frac{r - r_{\mathrm{s}}}{\alpha_{\pm}}\right)\cos(\xi) - \frac{r}{Rm}\varepsilon_{mn}^{(0)}\left(\frac{1}{\alpha_{\pm}}\right)\cos(\xi). \tag{16}$$

2.3. Field line tracing and poloidal Poincare maps

In order to verify the analytical flux-surface labeling introduced below, we first determine the flux surfaces by direct numerical integration of the magnetic field-line equations. The magnetic field lines, $\boldsymbol{\rho}(s) = \big(\rho_r(s), \rho_\theta(s), \rho_\varphi(s)\big) = (x(s), y(s), z(s))$ are defined by the equation

$$\frac{\mathrm{d}\boldsymbol{\rho}}{\mathrm{d}s} = \frac{\boldsymbol{B}(\boldsymbol{\rho}(s))}{|\boldsymbol{B}(\boldsymbol{\rho}(s))|}, \tag{17}$$

and we set $\mathrm{d}s = \sqrt{\mathrm{d}r^2 + r^2\mathrm{d}\theta^2 + (R_0 + r\cos\theta)^2\mathrm{d}\varphi^2} = \sqrt{\mathrm{d}x^2 + \mathrm{d}y^2 + \mathrm{d}z^2}$, so that $|\mathrm{d}\rho/\mathrm{d}s| = 1$ and the parameter s is the arc-length along the field line. The three differential equations (17) are solved numerically in Cartesian coordinates using a 4th-order Runge–Kutta, adaptive step-size method.

Figure 1 shows the poloidal cross section of the perturbed magnetic topology for the mode $(m, n) = (3, 2)$. The cross-section is calculated by determining the Poincarè surface of section (see, e.g. [32]) in the poloidal plane at $\varphi = 0$. The plasma parameters are chosen as relevant to ITER, major axis $R_0 = 6.2\,\mathrm{m}$, minor axis $\alpha = 1.9\,\mathrm{m}$, toroidal field on the magnetic axis $B_0 = 5.51\,\mathrm{T}$. The applied perturbation strength is $\varepsilon_{32}^{(0)} = 0.005$, corresponding to an island width of approximately 10 cm.

2.4. Flux-surface labeling

In order to calculate the volumes into which the EC wave energy is deposited, it is useful to have an analytical labeling Ω of the flux surfaces in the island region. For the general case of a perturbed non-axi-symmetric field, the field line equations

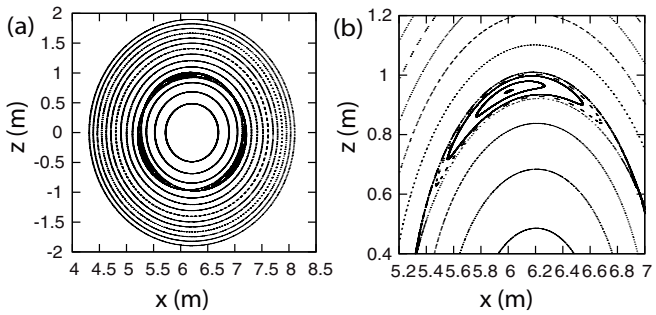

Figure 1. Poloidal cross section in Cartesian coordinates for the entire poloidal plane (*a*) and zoomed into the magnetic island area (*b*), for the (3, 2) mode and with ITER-like parameters.

are not integrable, in our case though of helical symmetry, the field line equations are integrable at the resonant surface, and can be well approximated analytically in a local neighborhood around the resonant surface (see [27, Chapter 9]).

The flux-surface labeling Ω basically is given by the helical flux ψ_{h} that can be calculated from the poloidal flux $\psi_{\mathrm{p}} = \psi_{\mathrm{p0}} + \psi_{\mathrm{p1}}$ through a canonical transformation from the toroidal variables $(\psi_{\mathrm{t}}, \theta)$ to the helical variables (ψ_{t}, ξ), with ξ the helical angle introduced above, and for practical reasons a Taylor expansion of ψ_{p0} is made in the radial direction (see [27, 29, 30, 34]). In our case then, the helical flux takes the form

$$\psi_{\mathrm{h}} = \frac{1}{2}\partial_{rr}\psi_{\mathrm{p0}}\Big|_{r_{\mathrm{s}}}(r - r_{\mathrm{s}})^2 + \frac{r}{m}\varepsilon_{mn}^{(0)}\left(1 + \frac{r - r_{\mathrm{s}}}{\alpha_{\pm}}\right)\cos(\xi). \tag{18}$$

So far, we have followed the derivation as performed in cylindrical coordinates, where the cylindrical components of the magnetic field are given as $(B_r^{(\mathrm{c})}, B_\theta^{(\mathrm{c})}) = (-[1/r]\,\partial_\theta\psi_{\mathrm{p}},\ \partial_r\psi_{\mathrm{p}})$. In toroidal coordinates though, we have $(B_r,\ B_\theta) = (-[1/\{rR\}]\,\partial_\theta\psi_{\mathrm{p}},\ [1/R]\,\partial_r\psi_{\mathrm{p}})$ (see equation (2)), so the background field and the perturbation are of the order of $R \approx R_0$ times smaller, and we have to correct Ω for this effect, since else the island width is over-estimated, as it was verified by comparison with the Poincare section shown in figure 1. Dividing moreover with $\partial_{rr}\psi_{\mathrm{p0}}|_{r_{\mathrm{s}}}$, the final expression for the flux-surface label is

$$\Omega = \frac{1}{2}(r - r_{\mathrm{s}})^2 + \frac{r}{r_{\mathrm{s}}}\Omega_{\mathrm{s}}\left(1 + \frac{r - r_{\mathrm{s}}}{\alpha_{\pm}}\right)\cos(\xi), \tag{19}$$

with

$$\Omega_{\mathrm{s}} = \frac{r_{\mathrm{s}}\varepsilon_{mn}^{(0)}}{mR_0\left(\partial_{rr}\psi_{\mathrm{p0}}\right)\Big|_{r_{\mathrm{s}}}} \tag{20}$$

the value of Ω on the separatrix (R_0 in the denominator is the correction factor from cylindrical to toroidal geometry), and the island half-width W approximately is

$$W = \sqrt{\frac{2r_{\mathrm{s}}\varepsilon_{mn}^{(0)}}{mR_0\left(\partial_{rr}\psi_{\mathrm{p0}}\right)\Big|_{r_{\mathrm{s}}}}}. \tag{21}$$

$\Omega = \Omega_{\mathrm{s}}$ defines the island separatrix, $-\Omega_{\mathrm{s}} \leqslant \Omega \leqslant \Omega_{\mathrm{s}}$ defines flux surfaces inside the island, while $\Omega > \Omega_{\mathrm{s}}$ defines

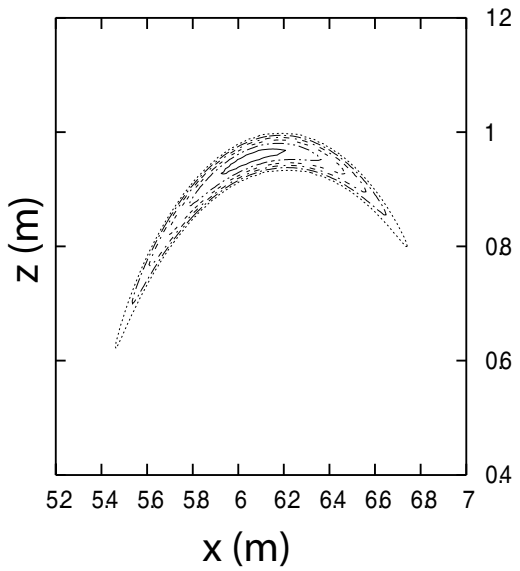

Figure 2. Contour plot of the flux-surface label Ω used in this work, equation (19).

flux surfaces outside the island. Ω can be normalized with a linear transformation in order to assume values in $[-1, 1]$ within the separatrix.

As mentioned, for a specific mode (m, n), the radial position r_s of the resonant surface can be determined by solving the equation $q(r_s) = m/n$. In order to improve again the coincidence of the flux-surface label and the Poincare plot in figure 1, we use a second-order correction in the inverse aspect ratio for the calculation of the safety factor, which yields

$$q^{(2)} = q\,\frac{R_0}{\sqrt{R_0^2 - r^2}} \tag{22}$$

(using the definition $q = (1/2\pi)\int_C (1/R)(B_\varphi/B_\theta) r\,\mathrm{d}\theta$, see, e.g. [26], inserting equations (4*a*)–(4*b*), and integrating). The use of $q^{(2)}$ in the determination of r_s yields a correction of the order of 2 cm to the value obtained from the large aspect ratio approximation.

Figure 2 shows the contour plot of Ω. The island width, shape and location are very close to the actual cross section shown in figure 1: the difference e.g. in the island width is of the order of 15%. Also note that the O- and the X-point are not exactly located at r_s, as explained in [33].

2.5. *Flattening of the plasma profiles*

The changes in the magnetic topology, as characteristic for an excited NTM, cause the plasma density and temperature to assume a constant value inside the separatrix of the island chain (by parallel conduction), and in consequence also the pressure profile is flattened [34, 35]. In order to model this alteration of the plasma profiles, we assume the density and temperature profiles to be parabolic functions outside the island, as in the unperturbed case, to be constant within the island region and to equal to the density and temperature values at the outer island boundary, and to be continuous at the inner island boundary. The expression for e.g. the electron density is

$$n_e(r) = \begin{cases} n_e(0) + [n_e(\alpha) - n_e(0)]\,\frac{r^2}{\alpha^2}, & r > r_s + w_\Delta, \\ n_e(0) + [n_e(\alpha) - n_e(0)]\,\frac{(r_s + w_\Delta)^2}{\alpha^2}, & |r - r_s| \leqslant w_\Delta, \\ n_e(0) + [n_e(\alpha) - n_e(0)]\,\frac{(r + 2w_\Delta)^2}{\alpha^2}, & r \leqslant r_s - w_\Delta, \end{cases}$$

where $n_e(0)$ and $n_e(\alpha)$ are the values of the density on the magnetic axis and at the plasma edge, respectively. An analogous expression is used for the profile of the electron temperature.

The local radial island half-width w_Δ depends on θ, φ (in the combination of ξ), it is determined through the local position of the separatrix. On the separatrix, Ω assumes the specific value Ω_s, and, for given θ, φ, the radial island borders r_1, r_2 are determined from the condition

$$\Omega(r, \xi) = \Omega_s,$$

which is a quadratic equation in $r - r_s$, with physically meaningful solution

$$w_\Delta = |r_{1,2} - r_s| = -\frac{\Omega_s \cos\xi}{\alpha_\pm} + \sqrt{\frac{\Omega_s^2 \cos^2\xi}{\alpha_\pm^2} - 2\Omega_s(\cos\xi - 1)}$$

(upon assuming $r/r_s = 1$ in the expression for Ω).

3. Ray tracing, wave absorption and current drive

The Hamiltonian equations for the ray propagation (ray equations) in the GO approach are [11, 12, 36]

$$\frac{\mathrm{d}\boldsymbol{k}}{\mathrm{d}\tau} = -\frac{\partial \mathcal{H}}{\partial \boldsymbol{r}}, \tag{23a}$$

$$\frac{\mathrm{d}\boldsymbol{r}}{\mathrm{d}\tau} = \frac{\partial \mathcal{H}}{\partial \boldsymbol{k}}, \tag{23b}$$

where $\boldsymbol{r}$ is the position of the ray, $\boldsymbol{k}$ is the wave vector, τ is a parameter denoting the length along the ray path and the Hamiltonian function $\mathcal{H}$ is given by the dispersion relation of the wave,

$$\mathcal{H} \equiv \det\left[\left(\frac{\omega}{c}\right)^2 \left(-k^2 \boldsymbol{I} + \boldsymbol{k}\boldsymbol{k}\right) + \boldsymbol{\epsilon}^h\right], \tag{24}$$

where $\boldsymbol{\epsilon}^h$ is the Hermitian part of the tensor that describes the plasma dielectric response to EC waves and $\boldsymbol{I}$ is the unit matrix. Assuming cold plasma propagation, one can adopt the cold plasma dielectric tensor [36], which leads to the expression for the Hamiltonian given in [37] and used here.

With $N_\parallel = \boldsymbol{N}\cdot\boldsymbol{B}/B$ and $N_\perp^2 = N^2 - N_\parallel^2$ the components of the refractive index $\boldsymbol{N} = c\boldsymbol{k}/\omega$ with respect to the magnetic field, the initial condition in magnitude N_0 for the ray is calculated from the dispersion relation of the specific wave mode and the values of the plasma parameters at the launch point. For waves in cold plasma, the equation $\mathcal{H} = 0$ determines N_0, with the Hamiltonian given in equation (24)

and [37]. The Cartesian components of the initial wave-vector may be expressed in terms of N_0 and the poloidal and toroidal injection angles, θ_l and φ_l, respectively,

$$k_{x0} = -\frac{\omega N_0}{c}\cos\varphi_l\cos\theta_l, \tag{25a}$$

$$k_{y0} = -\frac{\omega N_0}{c}\sin\varphi_l\cos\theta_l, \tag{25b}$$

$$k_{z0} = -\frac{\omega N_0}{c}\sin\theta_l. \tag{25c}$$

EC waves are strongly absorbed in a plasma when the Doppler-shifted wave frequency is close to a harmonic of the electron gyro-frequency [36],

$$\omega - k_{||}v_{||} - \frac{l\omega_c}{\gamma} = 0, \qquad (l = 0, \pm1, \pm2, \ldots). \tag{26}$$

The calculation of the wave absorption along the ray path can be performed either in terms of the linear absorption coefficient, as resulting from the wave-plasma energy balance [38], or in terms of the imaginary part of the wave vector, as determined from the mode-specific dispersion relation [15]. In the second treatment, which we follow here, the evolution of the total wave power P_w is determined by

$$\frac{dP_w}{d\tau} = -2\,\mathrm{Im}(\boldsymbol{k})\cdot\boldsymbol{v}_g\,P_w, \tag{27}$$

where $\boldsymbol{v}_g$ is the group velocity. Knowing the power of the ray along its path, the power dP_w deposited in a small radial interval can be calculated from equation (27), and division by the corresponding volume dV_s, which is contained between the two flux surfaces enclosing the radial interval, yields the absorbed wave power density.

The total driven current per wave power defines the current drive efficiency η_{CD}

$$\eta_{CD} = \frac{2\pi R_0 I_{CD}}{P_w}. \tag{28}$$

The computation of the ECCD efficiency can be performed either in terms of the linear adjoint method, or with quasi-linear Fokker–Planck (FP) models. The linear model, which we use here (following [16]), is based on a Green's function formulation, with the magnetic field approximated as a square well in order to obtain an analytic solution, and it includes the effects of trapped particles, ion–electron collisions and the poloidal variation of the collision operator.

For the accurate estimate of the wave absorption and current drive, the calculation of the plasma volume between two nearby flux surfaces is necessary, especially in the case where magnetic islands exist and the local topology is expected to affect quantitatively the power deposition. In order to determine the volume between flux surfaces, we first calculate the total volume V_s contained inside one flux surface,

$$V_s = -\frac{1}{n}\int_0^{2\pi n}\int_{\xi_1}^{\xi_2}\int_{r_1}^{r_2}(R_0 + r\cos\theta)\,r\,dr\,d\xi\,d\theta, \tag{29}$$

where $\xi = m\theta - n\varphi$ is the angle coordinate perpendicular to the helical line through the O-point [3], and r_1, r_2, ξ_1 and ξ_2 are the integration limits for r and ξ, respectively. The integration limits for a volume inside the island (normalized $\Omega < 1$) are determined as follows: A given flux surface has a unique value of Ω, say Ω_i. The equation $\Omega(r_s, \xi) = \Omega_i$ determines the limits ξ_1, ξ_2 in the helical (ξ) direction and at the radius $r = r_s$, and, for ξ in its integration interval $[\xi_1, \xi_2]$, the equation $\Omega(r, \xi) = \Omega_i$ determines the limits $r_1(\xi)$, $r_2(\xi)$ in the radial direction as a function of ξ. Using equation (19), we find

$$|r_{1,2} - r_s| = -\frac{\Omega_s\cos\xi}{\alpha_\pm} + \sqrt{\frac{\Omega_s^2\cos^2\xi}{\alpha_\pm^2} - 2(\Omega_s\cos\xi - \Omega_i)} \tag{30}$$

(assuming $r/r_s = 1$ in the expression for Ω), and

$$(\xi_1, \xi_2) = \left(2\pi - \arccos\left(\frac{\Omega_i}{\Omega_s}\right),\ \arccos\left(\frac{\Omega_i}{\Omega_s}\right)\right). \tag{31}$$

Note that the limits for the integral over θ take into account the number of poloidal windings needed for the island's flux tube to close on itself.

In order to compare the results from the island topology with those from the unperturbed case, we also need a flux-surface labeling for the latter, for which we make the assumption of a large aspect ratio, so that the integration limits simply are

$$(r_1, r_2) = \left(0, \alpha(\bar{\Omega} - 1)\right), \qquad (\xi_1, \xi_2) = (0, 2\pi), \tag{32}$$

with the obvious flux-surface label $\bar{\Omega} = 1 + r/\alpha$ (α is the minor radius), and with $n = m = 1$ in equation (29).

Finally, using equations (27) and (29), the absorbed power per unit volume can be evaluated as

$$\frac{dP_w}{dV_s} = \frac{dP_w/d\tau}{dV_s/d\tau}. \tag{33}$$

A ray tracing code has been developed for the computation of the EC wave propagation, as well as the power absorption and the driven current. The ray equations (23*a*)–(23*b*) and (24) are integrated with a 4th-order Runge–Kutta scheme, and the accuracy of the integration is controlled with an adaptive step-size method and by monitoring the deviation of $\mathcal{H}$ from zero. The wave absorption is calculated according to equation (27) using the routine DAMPBQ [15], which employs a weakly relativistic approximation to the plasma dielectric tensor. The driven current is calculated according to equation (28), with the current drive efficiency η_{CD} being computed in terms of the linear adjoint method (routine CURBA, [16]). Finally, the plasma volumes enclosed between two nearby flux surfaces are calculated by numerically integrating equation (29).

4. Numerical results

In this section, we present the numerical results on the effect of the magnetic island geometry on the EC wave propagation, power deposition and current drive. As described in section 2,

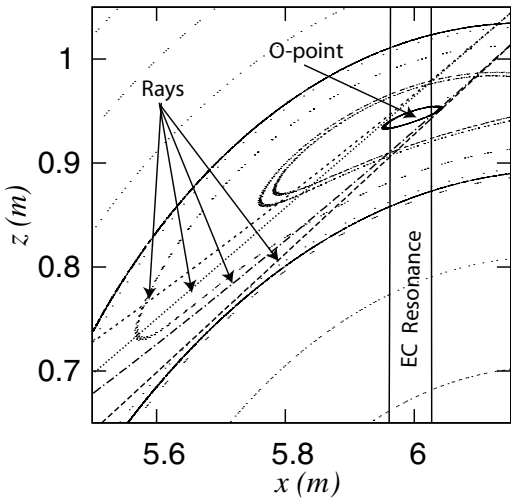

Figure 3. Poloidal cross section in Cartesian coordinates, zoomed into the resonance area, with two ray paths (short dashes and dashed–dotted) with different poloidal launching angles, for the (3, 2) mode, and for the unperturbed case (dotted and long dashes), and with ITER-like parameters.

we consider a perturbed magnetic equilibrium with an island chain, as generated by the NTM, and we include the effect of the flattening of the plasma density and temperature profiles in the islands' interior. The wave is injected from the outermost flux surface ($r = \alpha$), with the toroidal and poloidal launching angles such that the ray is targeted to a region very close to the O-point, and where the EC resonance is located around the center of the island.

We present results for the plasma and wave parameters as foreseen for ITER: The plasma major and minor radii are $R_0 = 6.2\,\mathrm{m}$ and $\alpha = 1.9\,\mathrm{m}$, respectively, the magnetic field on the magnetic axis is $B_0 = 5.51\,\mathrm{T}$, the electron density at the plasma center and edge is $n_\mathrm{e}\,(0) = 10^{20}\,\mathrm{m}^{-3}$ and $n_\mathrm{e}\,(\alpha) = 10^{19}\,\mathrm{m}^{-3}$, respectively, and the electron temperature at the center and edge is $T_\mathrm{e}(0) = 10\,\mathrm{KeV}$ and $T_\mathrm{e}(\alpha) = 1\,\mathrm{KeV}$, respectively. The wave frequency is $\omega/2\pi = 160\,\mathrm{GHz}$, corresponding to the fundamental cyclotron frequency, with assumed O-mode polarization, while the injected wave power is $P_{\mathrm{w}0} = 10\,\mathrm{MW}$. Regarding the parameters of the NTM generating the magnetic islands, we throughout consider the mode (3, 2), with a magnetic perturbation strength $\varepsilon_{32}^{(0)} = 5 \times 10^{-3}$ and slopes $\alpha_+ = \alpha_- = 12$ (a typical value from [30]), which corresponds to a symmetric island width of approximately 10 cm (the exact width depends on the island's location in the poloidal plane, due to the inhomogeneity of the background magnetic field).

In figure 3, we show ray paths in the presence of the NTM for two different poloidal launching angles. The figure also shows the corresponding ray paths in the absence of the NTM, i.e. in the unperturbed equilibrium, for a comparison of the two cases. The waves are injected at the poloidal angle $\theta_l = 30^\circ$, with the toroidal launching angle being $\varphi_l = 0^\circ$. For the assumed profiles of $\boldsymbol{B}$, n_e, T_e, and the value of ω, the region of the EC resonance is located around $R = 6\,\mathrm{m}$ and marked in figure 3 by two vertical lines.

The ray propagation is not much affected by the magnetic field of the island, since the relative magnetic perturbation strength ($\sim 10^{-3}$) is small. However, during the passage of the ray through the island region, a deviation of the propagation path from the unperturbed case appears, which increases along the path (see figure 3). This deviation is caused by wave refraction and is due to the different density profiles in the two cases (the density is constant within the island in the perturbed case). In the part of the ray path within the island region, and before reaching the O-point, the deviation is in general very small (of the order of a few mm). Since usually all the wave power is deposited inside the resonance area, the full deviation through the entire island can play a significant role only in the case of incomplete absorption in the island region. Also, with certain launching angles or island locations different from the one shown here, the ray might travel a longer distance inside the island before reaching the resonance, and the deviation might become comparable to the maximum misalignment allowed for efficient NTM stabilization (2–3 cm) [7]. A significant deviation of the ray may also be caused not by the target island itself, but by a secondary island at a larger radius that the ray happened to cross before arriving at the target island (see, e.g. [39] for EC wave scattering by plasma density fluctuations).

To compute the power deposition, it is required to calculate the volumes $\mathrm{d}V_\mathrm{s} = |V_\mathrm{s}(\tau + \mathrm{d}\tau) - V_\mathrm{s}(\tau)|$ between successive flux surfaces crossed by the ray within the resonance region, with $\mathrm{d}\tau$ being a step chosen here to be equivalent to 10 electron Larmor radii (1 electron Larmor radius at ITER is around $5 \times 10^{-5}\,\mathrm{m}$). The volumes $V_\mathrm{s}(\tau)$ and their differences $\mathrm{d}V_\mathrm{s}$, into which the power $\mathrm{d}P_\mathrm{w} = P_\mathrm{w}(\tau + \mathrm{d}\tau) - P_\mathrm{w}(\tau)$ is deposited, are shown in figure 4 for both cases, the perturbed and the unperturbed one, respectively. It is obvious that the presence of the island has the consequence that the power is deposited into volumes smaller than those of the unperturbed case, which in turn leads to larger values of the absorbed power density. Varying $\mathrm{d}\tau$ over a wide range of values did not alter the results presented below, the dependences of the values of $\mathrm{d}V_\mathrm{s}$ and $\mathrm{d}P_\mathrm{w}$ on $\mathrm{d}\tau$ are complementary.

As an additional benchmark for the accuracy of the numerical computation in general, as well as for the computation of the absorbed power per unit volume, we determined the total absorbed wave power $P_\mathrm{total} = \int (\mathrm{d}P_\mathrm{w}/\mathrm{d}V_\mathrm{s})\mathrm{d}V_\mathrm{s}$ numerically, which should be constant and equal in all cases, with or without magnetic perturbation. This is illustrated in figure 5, where the integrand $\mathrm{d}P_\mathrm{w}/\mathrm{d}V_\mathrm{s}$ is shown as a function of the flux-surface volume V_s (integration variable) for two different cases, and, as in the example, the area under the curve $\mathrm{d}P_\mathrm{w}/\mathrm{d}V_\mathrm{s}$ was indeed found to be equal in all cases considered.

As explained above, with a magnetic island present, the wave power is absorbed in smaller flux-surface volumes, with the direct consequence that the power deposition and current drive are strongly increased. This is shown in figure 6 for a typical case, where the wave is injected at the poloidal angle $\theta_l = 30^\circ$ and the toroidal launching angle is 0°. In the presence of an NTM, the absorbed power density is found to be nearly 3 times larger than the one in the unperturbed case. The driven current density has a similar behavior, attaining a value of more than 3 times larger than in the absence of the NTM perturbation.

In figure 7, we show two purely geometrical effects on the power deposition, in cases where the ray is extremely well

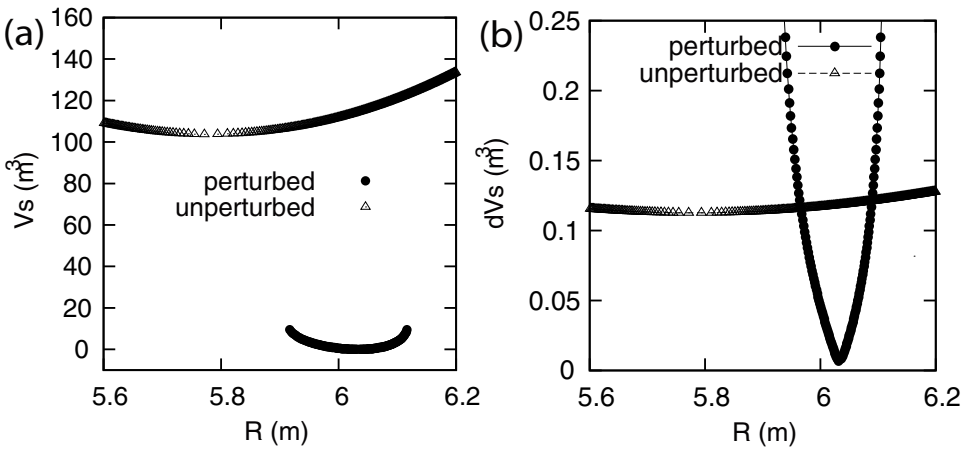

Figure 4. For the two cases of propagation with a (3, 2) NTM mode present and without a perturbation, we show the volumes V_s of the flux surfaces (a) and the volume differences $\mathrm{d}V_s$, into which the wave power $\mathrm{d}P_w$ is deposited (b). In the perturbed case, the volumes are shown only when the ray is within the island.

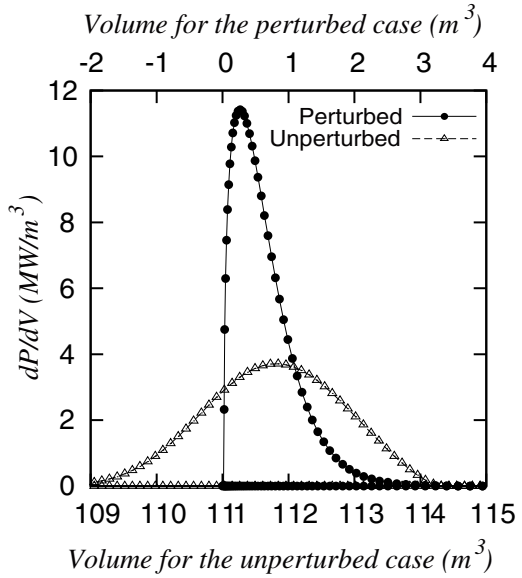

Figure 5. Visualization of the 'conservation' of the total absorbed wave power: Power deposition per unit volume $\mathrm{d}P_w/\mathrm{d}V_s$ as a function of the flux-surface volume V_s, for the perturbed and the unperturbed case.

targeted and passes very close by the O-point. In the case of figure 7(a), the power deposition would have reached its maximum (right peak in the figure) slightly before the ray is closest to the O-point on its path, yet it then approaches the O-point and enters the innermost (on its path) flux surface, with the path inside this flux-surface volume being substantially longer than in the flux surfaces before and after, as illustrated by the dashed–dotted ray path in figure 8. There is thus more time for interaction and power-deposition, and $\mathrm{d}P_w$ is substantially increased in this flux surface, which causes the secondary, left peak to appear in figure 7(a). In the case of figure 7(b), the ray enters the innermost volume, and, as illustrated by the dashed ray-path in figure 8, spends a relatively long time in the volume, the volume moreover is small, and, with the O-point lying at the center of the resonance region, a strongly increased central peak appears in figure 7(b). As stated, these two cases occur only for very well targeted rays, they thus are exceptional cases and the probability for them to be observed in experiments must be expected to be very small.

Finally, we investigate the effect of the toroidal launching angle φ_l on the power deposition and the driven current, by applying the toroidal launching angles $\varphi_l = -5^\circ$, 0°, 5° and 10°, and without changing any of the other parameters. The results are summarized in table 1. For a toroidal launching angle of 5°, the driven current is almost zero since the ray crosses the island tube perpendicularly, and hence there is no component of the driven current parallel to the magnetic field. Starting thus from $\varphi_l = -5^\circ$, the driven current density is positive, vanishes at $\varphi_l = 5^\circ$, and becomes again large, but negative now, at $\varphi_l = 10^\circ$. Depending on φ_l, the driven current density in the perturbed case reaches values up to 2–4 times larger than in the unperturbed case.

5. On the effect on NTM stabilization

Based on the results of the previous section, the question arises whether the effects of the island geometry on the ECCD efficiency also play a significant role in NTM stabilization. Here, only a preliminary investigation of this issue is made. The NTM dynamics can sufficiently be described by the modified Rutherford equation [1, 9], which is the established model for the dynamic evolution of NTMs. In the case of classical TMs, only the contribution of the ohmic current plays a role, whereas for NTMs other currents that flow in the island region, as appearing in neoclassical transport, need to be taken into account, too. For our analysis, it is sufficient to assume that the main current that affects the island evolution, in addition to the stabilizing ECCD, is the bootstrap current.

In this framework, the modified Rutherford equation takes the form [8]

$$\frac{\tau_r}{r_s}\frac{\mathrm{d}W}{\mathrm{d}t} = r_s\left(\Delta' + \Delta'_{sat} + \Delta'_{BS} + \Delta'_{CD}\right), \qquad (34)$$

where W is the half-width of the magnetic island, $\tau_r = 936.4\, r_s^2$ is the resistive time-scale of the plasma, Δ' is the classical

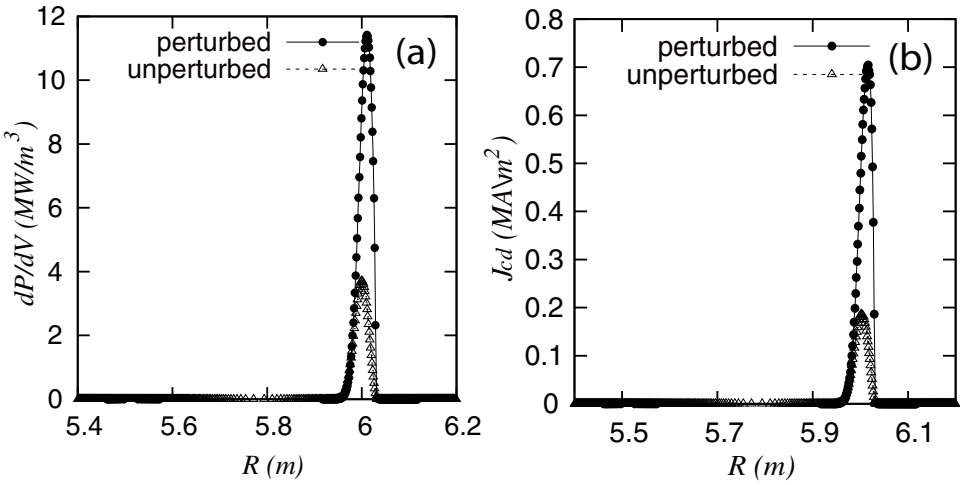

Figure 6. Deposited wave power per unit volume $\mathrm{d}P_\mathrm{w}/\mathrm{d}V_\mathrm{s}$ (a) and the corresponding driven current density (b) as a function of the major radius R, for the cases of propagation with a (3,2) NTM mode present and without perturbation.

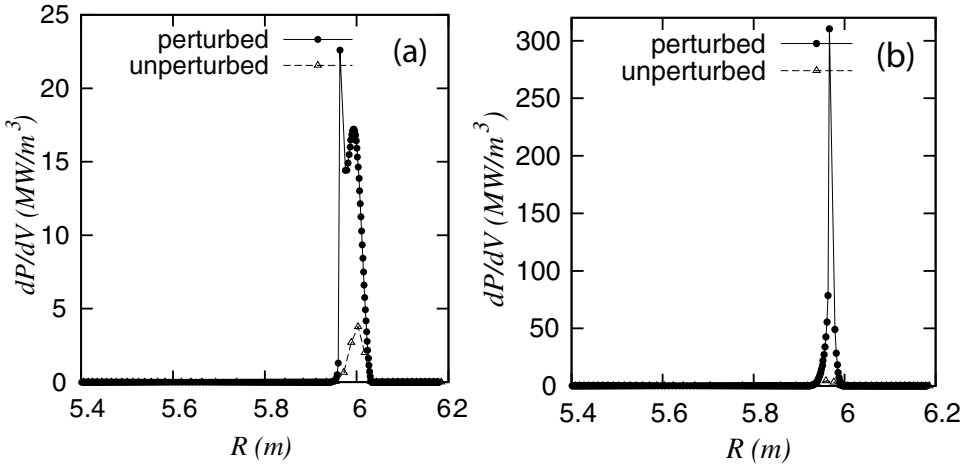

Figure 7. Power deposition profile (a) when the ray is closest to the O-point after the main peak, and (b) when the ray crosses the innermost flux surface and the O-point lies at the peak region of the resonance.

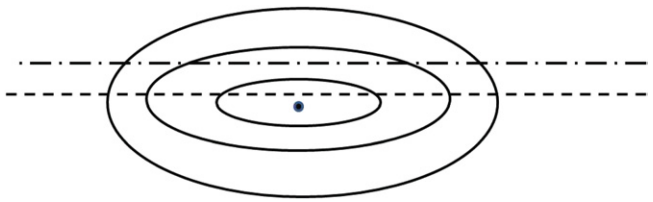

Figure 8. Sketch of the innermost flux surfaces (solid lines) near the island's O-point (solid dot) and two possible ray paths (dashed and dotted–dashed lines).

TM stability index, Δ'_sat is the stability index connected to the non-linear island saturation and the structure of the magnetic equilibrium, Δ'_BS is the stability index corresponding to the bootstrap current, which becomes significant for high values of the plasma pressure, and Δ'_CD is the term which represents the stabilizing effect of the ECCD on the magnetic island. The four stability indices are defined as [1, 30, 40, 41]

$$\Delta' = \left(\partial_r \psi_{\mathrm{p1}} \Big|_{r_\mathrm{s}+} - \partial_r \psi_{\mathrm{p1}} \Big|_{r_\mathrm{s}-} \right) \frac{1}{\psi_{\mathrm{p1}} \Big|_{r_\mathrm{s}}}, \tag{35a}$$

$$\Delta'_\mathrm{sat} = -\frac{W}{2.44 a_\mathrm{J}^2}, \tag{35b}$$

$$\Delta'_\mathrm{BS} = \frac{\sqrt{\epsilon_\mathrm{A}}\beta_\mathrm{P}}{W} \frac{L_q}{L_p} \left(\frac{W^2}{W^2 + W_\mathrm{d}^2} + \frac{W^2}{W^2 + 28 W_\mathrm{b}^2} - \frac{W_\mathrm{pol}^2}{W^2} \right), \tag{35c}$$

$$\Delta'_\mathrm{CD} = -0.31 L_q \frac{\mu_0 j_\mathrm{CD0}}{2 B_\mathrm{p}} \left[\frac{34 d_\mathrm{CD}}{W^2} g_\mathrm{wd} + \frac{4\sqrt{\pi}}{d_\mathrm{CD}} (1 - g_\mathrm{wd}) \right]. \tag{35d}$$

In the above, the form of Δ' follows the one given in [30], a_J represents the length of variation of the equilibrium current density (see [40] for a discussion of Δ'_sat), ϵ_A is the aspect ratio of the tokamak, $\beta_\mathrm{P} = 2\mu_0 P/B^2$ is the ratio of the plasma pressure over the magnetic pressure, L_q and L_p are the shear lengths of the safety factor and the plasma pressure, μ_0 is the permeability of free space and B_p the poloidal magnetic field, j_CD0 and g_wd are defined below, d_CD is the wave power deposition width and W_d ,W_b, W_pol are the characteristic threshold values for the island width [8]: W_d is the critical width for NTM destabilization, W_b is the width below which

Table 1. Power deposition dP_w/dV_s and driven current density J_{CD0} for different toroidal launching angles ϕ_l, for both the NTM-perturbed and the unperturbed case, respectively.

ϕ_l	dP_w/dV_s (MW m^{-3})		J_{CD0} (MA m^{-2})	
	Unperturbed	Perturbed	Unperturbed	Perturbed
-5°	3.03	10.48	0.70	2.78
0°	3.70	11.40	0.19	0.70
5°	4.50	13.95	0.001	0.002
10°	8.26	26.97	−0.50	−1.81

the banana orbits contribute significantly to the bootstrap current and W_{pol} is the width below which the electron-ion polarization current, generated in response to the diamagnetic island rotation, is significant.

From the definition of Δ' and the form of ψ_{p1} in equation (14), it follows that

$$\Delta' = \left(\partial_r \psi_{p1}\Big|_{r_s+} - \partial_r \psi_{p1}\Big|_{r_s-}\right) \frac{1}{\psi_{p1}\Big|_{r_s}} = \frac{1}{\alpha_+} - \frac{1}{\alpha_-} \tag{36}$$

(see, [30]; for a detailed analysis of Δ' see, e.g. [29]).

Apart from the total driven current, two more characteristics of the ECCD are important for NTM stabilization, the spatial distribution of the driven current density and its efficiency in replacing the missing bootstrap current. The current density is assumed here to exhibit a Gaussian distribution in space,

$$j_{CD} = j_{CD0} \exp\left[-\frac{(r - r_s - r_{mis})^2}{d_{CD}^2}\right], \tag{37}$$

where r_{mis} is the small distance of misalignment of the ECCD deposition center from the island's O-point. The efficiency of the ECCD in stabilizing the NTM is described by the parameter g_{wd} [8],

$$g_{wd} = \begin{cases} 0.3\frac{W}{d_{CD}}, & \frac{W}{d_{CD}} < 2, \\ \exp\left(-\frac{d_{CD}}{W}\right), & \frac{W}{d_{CD}} > 2. \end{cases} \tag{38}$$

The phase diagram of the modified Rutherford equation, which actually is a visualization of the island's growth dynamics, is shown in figure 9 for two indicative cases relevant to the mode (3, 2). We compare the results for two different toroidal launching angles, -5° and 0°, each for the three different cases of (i) no ECCD applied, (ii) ECCD applied but calculated in the absence of the island and (iii) ECCD applied and calculated by taking into account the island topology. For the plasma and wave parameters we use the same ITER-relevant values as in the previous section, and for the parameters newly introduced in this section we set $\beta_P = 0.5$, $L_q/L_p = 1$, $W_d = 0.01 r_s$, $W_b = 0.02 r_s$, $W_{pol} = 0.015 r_s$, $r_{mis} = 1$ cm, $a_J = 1.9$ m, $w_{sat} = 0.2$ m [1], and the value of the driven current density (j_{CD0}) is taken from table 1.

For a toroidal launching angle of 0°, figure 9(*a*) shows that (i) without ECCD applied the island is unstable to grow in a wide range of widths, (ii) with ECCD applied but calculated without taking the island topology into account, there is still a region of unstable widths, with dW/dt small and positive for intermediate and large size islands and (iii) with ECCD applied and calculated by taking the island geometry into account, there is an effective NTM stabilization, since dW/dt has becomes negative for all widths, being largest in magnitude in case (iii). The reason for the higher effectiveness in case (iii) is the peaking of the ECCD profile when the island topology is taken into account, as the ECCD density is nearly 3.5 times larger than the one calculated in the unperturbed equilibrium, and also the deposition width is 1.2 times smaller (see table 1).

As the toroidal launching angle increases in magnitude, the situation becomes even more favorable for stabilization, as visualized in figure 7(*b*) for $\phi_l = -5^\circ$. In this case, the values of dW/dt are still negative but larger in magnitude than for $\phi_l = 0^\circ$. This effect could serve as a power economy policy, because less ECCD is required for stabilization if the toroidal launching angle is made as large as technically possible. Note though that, according to table 1, the minimum driven current density is attained at $\phi_l = 5^\circ$, due to three-dimensional scattering effects in the ray propagation, and it actually is the toroidal angle of incidence on the resonance region that should be made as large as possible in order to gain efficiency. In the case $\phi_l = -5^\circ$, there is also an increase of the margins of acceptable ECCD deposition misalignment, since the large value of the ECCD density may compensate a reduction of the driven current due to a deposition further away from the O-point.

6. Summary and discussion

The NTMs are expected to be a major issue for ITER operation, since a high plasma pressure is required for an effective fusion device, and under such conditions both the (2, 1) and (3, 2) modes appear and persist. Currently, the most efficient technique for the stabilization and control of NTMs is to deposit ECCD very close to the island's O-point, in order to replace the missing bootstrap current. Up to now, this issue has been analyzed by ignoring any effects from the island topology on the efficiency of the wave absorption and current drive, in accordance with the assumption that the perturbations in the magnetic field are of very small amplitude.

In this paper, we have studied the EC wave propagation, absorption and current drive in the presence of NTMs (magnetic islands), using the ray tracing method and a model for a tokamak magnetic field that includes islands, and we also have investigated the effects of the island geometry on the NTM dynamic evolution.

The analytical model for the magnetic islands and the tokamak background field are more realistic than the standard models adopted so far in the literature, they just have not yet been compared with experimental data (this effort is under way). We also have introduced a correction for toroidal geometry to the flux-surface labeling in the island region, so that the island is represented in a realistic way and the precision in the determination of the flux-surface volumes is improved, which in turn leads to increased accuracy in the calculation of the power deposition.

Our main results imply that (*a*) in most cases, the propagation until the O-point is little affected by the magnetic

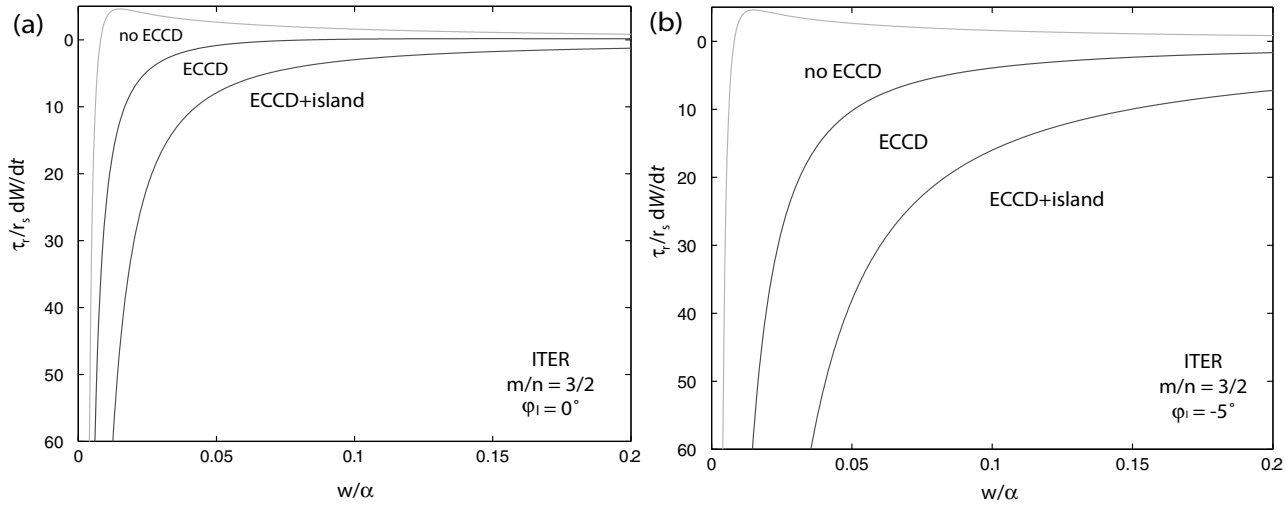

Figure 9. Phase diagram of the modified Rutherford equation for $m/n = 3/2$ and $\phi_l = 0^\circ$ (a), $\phi_l = -5^\circ$ (b).

island topology, due to the very small magnitude of the perturbation, with any effects owed to the flattening of the plasma pressure within the island region. (b) The absorbed wave power and the driven current are affected significantly by the island geometry, namely enhanced, the energy is absorbed and redistributed by the plasma particles in flux-surface volumes much smaller than the ones in an axi-symmetric topology. (c) The use of an island topology allows a more accurate estimate of the NTM stabilization effect of ECCD, and it turns out that the increased ECCD peaking in the islands topology results in a much better efficiency of NTM stabilization, i.e. stabilization can be achieved with less wave power than the one estimated in axisymmetric geometry.

The driven current depends on two main parameters, the geometry of the flux surfaces and the toroidal launching angle. The driven current density increases with increasing toroidal launching angle, since the component of the wave which is parallel to the magnetic field becomes larger. The island geometry affects very much the driven current in that it determines the deposition volumes, and already small deviations of the ray from the O-point lead to a significantly reduced driven current, possibly below the desired level, which in turn may jeopardize a stabilization effort. Apart from the island magnetic field structure, which plays a crucial role for the wave deposition profiles, the presence of an NTM introduces a flattening of the plasma pressure within the island region, which is a major difference to the plasma density and temperature profiles in the axi-symmetric case.

Concerning the basic assumptions made in our modeling approach, we mention that the routines for the computation of the wave propagation, absorption and current drive are based on linear methods that do not account for (a) wave diffraction, (b) trapping of particles in the island chain or (c) nonlinear effects due to the very large values that the absorbed power density may attain. These issues are under current study in order to improve our model. Second, the island dynamics were described in terms of a version of the modified Rutherford equation that includes a simplification in the expression for the classical stability index Δ'. In principle, Δ' should be computed using the exact equilibrium current profile in a fully toroidal geometry. This is a very complicated task, which is still under investigation. Since our work is focused on the effect of the island geometry on the EC absorption and current drive, making also a primary assessment for the effect on the NTM stabilization, we adopted the simple model for Δ' described in [30] (see also [29]), which makes the form of the Rutherford equation consistent with the perturbation in the poloidal flux that we used in order to set up the island topology. Finally, the effect of the island geometry on the NTM dynamics has been studied in terms of a quasi-self-consistent coupling of the wave propagation solver to the equation governing the island dynamics. A feasibility study for the development of a fully self-consistent model, either in terms of changing the magnetic topology at certain time slices during the wave propagation, or with ray tracing in time-dependent fields, is under way.

Other studies have been made [19–21] that were focused on the effect of local transport on the ECCD efficiency, using a quasi-linear Fokker–Planck approach or test-particle simulations, and simulating the ECCD process in more detail than with the linear models used here, yet without accounting for the characteristics of the EC wave propagation and absorption. These studies find that, in the presence of magnetic islands, the transport properties are such that the current drive efficiency is much enhanced compared with the axisymmetric case, they thus also lead to a different estimate of the ECCD required for stabilization, in accordance with the results presented here.

In conclusion, the NTM appearance and evolution are likely to be an important issue for ITER's optimal performance, the prospects though of controlling them using radio-frequency waves to drive a current close to the rational surface where the instability appears, also in the form of early ECCD application with the scope of manipulating an island's seeding mechanism, look promising. Issues that need to be investigated further include (a) modeling of the wave propagation with the plasma response computed in terms of the full particle dynamics in

the non-axisymmetric fields. (*b*) The effect of the ECCD on the background magnetic equilibrium, which may have been underestimated in the computations performed up to now. (*c*) The propagation, absorption and current drive in scenarios where the stabilization of multiple (overlapping or not) NTMs is required.

Acknowledgments

The authors would like to thank E Poli, A Lazaros, K Hizanidis, A K Ram and Y Kominis for helpful discussions, as well as the two anonymous referees for their valuable comments.

This work was sponsored by the European Fusion Programme (Association EURATOM-Hellenic Republic) and the Hellenic General Secretariat of Research and Technology. The sponsors do not bear any responsibility for the contents of this work.

References

[1] Hegna C C and Callen J D 1997 *Phys. Plasmas* **4** 2940
[2] LaHaye R J 2006 *Phys. Plasmas* **13** 055501
[3] Wilson H R 2008 *Trans. Fusion Science Technol.* **53** 152
[4] Miyamoto K 2004 *Plasma Physics and Controlled Nuclear Fusion* (Berlin: Springer)
[5] Carrera R, Hazeltine R D and Kotschenreuther M 1986 *Phys. Fluids* **29** 899
[6] LaHaye R J, Prater R, Buttery R J, Hayashi N, Isayama A, Maraschek M, Urso L and Zohm H 2006 *Nucl. Fusion* **46** 451
[7] Zohm H, Gantebein G, Leuterer F, Maraschek M, Poli E, Urso L and the ASDEX Upgrade Team 2007 *Plasma Phys. Control. Fusion* **49** B341
[8] Urso L 2009 Modelling and experiments on NTM stabilisation at ASDEX upgrade *PhD Thesis* Ludwig-Maximilians Universitaet Muenchen
[9] Rutherford P H 1973 *Phys. Fluids* **16** 1903
[10] Lazaros A, Maraschek M and Zohm H 2007 *Phys. Plasmas* **14** 042505
[11] Bernstein I B 1975 *Phys. Fluids* **18** 320
[12] Friedland L and Bernstein I B 1980 *Phys. Rev.* A **22** 1680
[13] Mazzucato E 1989 *Phys. Fluids* B **1** 1855
[14] Pereverzev G V 1998 *Phys. Plasmas* **5** 3529
[15] Westerhof E 1989 Implementation of Toray at JET *Rijnhuizen Rep.* RR-89-183
[16] Cohen R H 1987 *Phys. Fluids* **30** 2442
[17] Karney F F 1986 *Comput. Phys. Rep.* **4** 183
[18] Prater R *et al* 2008 *Nucl. Fusion* **48** 035006
[19] Hamamatsu K, Takizuka T, Hayashi N and Ozeki T 2007 *Plasma Phys. Control. Fusion* **49** 1955
[20] Rosa P R and Ziebell L F 2008 *Plasma Phys. Control. Fusion* **50** 095002
[21] da Silva Rosa P R and Giruzzi G 2000 *Plasma Phys. Control. Fusion* **42** 755
[22] Boozer A 2004 *Rev. Mod. Phys.* **76** 1071
[23] Abdullaev S S 2006 *Construction of Mappings for Hamiltonian systems and their applications* (Berlin: Springer)
[24] Balescu R 1988 *Transport Processes in Plasmas: 2. Neoclassical Transport Theory* (Amsterdam: North-Holland)
[25] Misguish J H 2001 *Phys. Plasmas* **8** 2132
[26] Wesson J 2004 *Tokamaks* (Oxford: Clarendon)
[27] Hazeltine R D and Meiss J D 1992 *Plasma Confinement* (WA: Addison-Wesley Redmond)
[28] Biskamp D 2000 *Magnetic Reconnection in Plasmas* (Cambridge: Cambridge University Press)
[29] Militello F, Hastie R J and Porcelli F 2006 *Phys. Plasmas* **13** 112512
[30] Ren C, Callen J D, Gianakon T A, Hegna C C, Chang Z, Fredrickson E D, McGuire K M, Taylor G and Zarnstorff M C 1998 *Phys. Plasmas* **5** 450
[31] Urso L, Zohm H, Isayama A, Maraschek M, Poli E, ASDEX Upgrade Team and JT-60 Team 2010 *Nucl. Fusion* **50** 025010
[32] Lichtenberg A J and Lieberman M A 1992 *Regular and Chaotic Dynamics* (Berlin: Springer)
[33] White R B and Monticello D A 1977 *Phys. Fluids* **20** 800
[34] Fitzpatrick R 1995 *Phys. Plasmas* **2** 825
[35] Hayashi N, Ozeki T, Hamamatsu K and Takizuka T 2004 *Nucl. Fusion* **44** 477
[36] Stix T H 1992 *Waves in Plasmas* (Berlin: Springer)
[37] Poli E, Peeters A G and Pereverzev G V 2001 *Comput. Phys. Commun.* **136** 90
[38] Bornatici M 1983 *Nucl. Fusion* **23** 1153
[39] Tsironis Ch, Peeters A G, Isliker H, Strintzi D, Chatziantonaki I and Vlahos L 2009 *Phys. Plasmas* **16** 112510
[40] Militello F and Porcelli F 2004 *Phys. Plasmas* **11** L13
[41] Westerhof E *et al* 2007 *Nucl. Fusion* **47** 85